

ESD-based Crowbar for Mitigating DC-link Variations in a DFIG-based WECS

Muhammad Arif Sharafat Ali, Khawaja Khalid Mehmood, Ji-Soo Kim, Chul-Hwan Kim

Abstract—A doubly-fed induction generator (DFIG) is highly vulnerable to the grid faults that induce large electromotive force in its rotor circuit. Large penetration of DFIG-based wind energy conversion systems (WECS) into existing power systems raises the importance of low-voltage ride-through (LVRT) capability of the DFIG. Motivated by the above arguments, this study focuses on the mitigation of DC-link voltage variations with the help of a crowbar based on an energy storage device that supports the DFIG to enhance its LVRT capability during grid faults. The proposed design is incorporated into a combination of a rotor-side crowbar to limit the rotor over-currents. Moreover, an efficient synchronization mechanism is also proposed for smooth connection of a DFIG with the grid to minimize the startup inrush currents. The overall proposed schemes are intended for a 1.5 MW DFIG-based WECS. Extensive simulations are carried out in Simulink/Matlab to validate the performances of the proposed schemes. The results confirm that the proposed control schemes are capable to cope with DC-link voltage variations and rotor over-currents within safe operating limits and the smooth connection of a DFIG with the grid as well without significant inrush currents.

Keywords: Crowbar, doubly-fed induction generator, energy storage device, low-voltage ride-through, vector control, wind energy conversion system.

I. INTRODUCTION

A rapid increase in the penetration of wind power plants into existing power infrastructure raises the reliability and stability concerns of power systems [1]. Under aforesaid circumstances, it is unavoidable to minimize the negative impacts of large-scale wind power integration. Different countries have made efforts to resolve this critical issue and revised their grid codes by imposing the low-voltage ride-through (LVRT) requirements in order to keep the power system stability intact [2]. LVRT describes the capability of the wind energy conversion systems (WECS) to remain coupled to the grid during faults and also to provide certain reactive power for transient voltage recovery [3].

Recently, doubly-fed induction generators (DFIGs) are the most popular type for WECSs due to their variable-speed operation, high efficiency, and reduced capacity of power

electronics converters [4]. Motivated by the above arguments and the upsurge in the cost of the permanent magnetic material, DFIGs have competitive advantages over permanent-magnet synchronous generators. Having a direct connection to the grid, a DFIG is highly susceptible to grid disturbances, mainly voltage dips. During the fault, a large electromotive force (EMF) induces in the rotor circuit due to reduced capacity of the rotor-side converter (RSC) and DC-link voltage limitation [5]. As a result, both the RSC and grid-side converter (GSC) are likely to experience over-currents and to cause transient over-voltages in the DC-link that connects the RSC and GSC.

To address the aforementioned concerns and to improve the LVRT capability of a DFIG-based WECS, extensive research has been conducted, and numerous technical solutions are available in literature. These solutions can be primarily classified into two main groups: (1) modification of DFIG converter control systems and (2) auxiliary hardware applications. Several modified control methods are presented in [3], [4], [6]–[9] such as flux-linkage control [3], improved RSC control [4], flux magnitude and angle control [6], negative-sequence current regulation [7], enhanced reactive power-based LVRT strategy [8], and demagnetization current method [9]. Application of an auxiliary hardware such as crowbar protection is the most common in present wind turbines (WTs) [5], [10]. Recently, the application of fault current limiters was established as an effective solution for enhancement of LVRT capability [2], [11]. Applications of some other hardware are also suggested such as application of a STATCOM [12] and an energy storage device [1].

This study concentrates the LVRT capability of a DFIG-based WECS during severe grid voltage dips and suggests a scheme based on crowbar auxiliary controls. Under the proposed scheme, rotor crowbar resistors are coupled to the RSC in parallel with a three-phase rotor circuit breaker (RCB) to make the rotor-side crowbar (RSCB), whereas the DC-link crowbar (DLCB) based on an energy storage device (ESD) which is a nickel-metal-hydride battery, is connected in parallel to the DC-link capacitor. Moreover, an efficient synchronization algorithm is also developed to minimize the startup inrush currents and to ensure the smooth and stable connection for grid-tied applications. This study focuses not only on mitigating the rotor-side over-currents, but also enhancing the DC-link response in support of a grid during voltage dips. Numerical simulations are performed not only to confirm the effectiveness, but also to verify the enhanced LVRT capability of a DFIG-based WECS with the support of the proposed control scheme.

The main contributions of this work can be summarized as

This work was supported by the National Research Foundation of Korea (NRF) grant funded by the Korea government (MSIP) (No. 2018R1A2A1A05078680).

The authors are with the Department of Electrical and Computer Engineering, Sungkyunkwan University, Suwon City, 440-746, Republic of Korea.
Email: sharafat@skku.edu; khalidmzd@skku.edu; kjs7107@naver.com; chkim@skku.edu

follows:

- A synchronization mechanism is developed for a smooth and stable connection of a DFIG-based WECS to the grid with trivial startup inrush currents.
- An efficient and effective control scheme is designed to cater for the effects of rotor-side current transients and DC-link voltage fluctuations to enhance the LVRT capability of a DFIG-based WECS during grid voltage dips.

The remainder of this paper is organized as follows. In Section II, a brief overview of the studied grid-connected WECS is presented. A comprehensive review of the studied WECS and the modelling of RSC and GSC controls are incorporated in Section III. Section IV describes the proposed control schemes for grid synchronization and LVRT capability enhancement during grid voltage dips. Simulation results and analyses are provided in Section V. Finally, Section VI presents the concluding remarks.

II. OVERVIEW OF THE STUDIED GRID-CONNECTED WECS

The configuration of the studied grid-connected WECS is presented in Fig. 1, which contains a variable-speed wind turbine (VSWT), DFIG, RSC, RSCB, intermediary DC-link circuit, DLCB, GSC, and control system. Detailed mathematical modelling of the studied DFIG-based WECS including the control system is presented in a subsequent section.

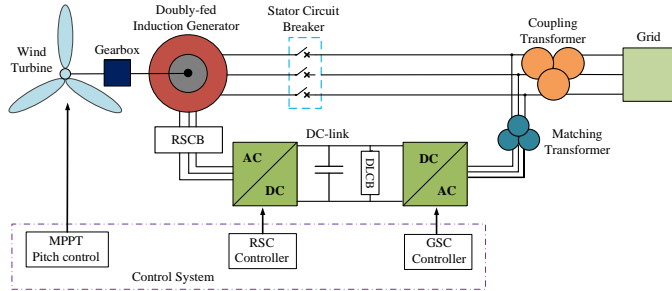


Fig. 1. Configuration of the studied grid-connected WECS.

Here, the stator of the generator is directly coupled to the grid via a high-voltage step-down transformer and a three-phase stator circuit breaker (SCB), whereas the rotor is integrated indirectly through back-to-back (BTB) pulse-width modulation (PWM) converters. BTB converters control the energy flow from machine to the grid and vice versa. The DC-link voltage should be suitably controlled to keep it stable to realize the LVRT capability of a DFIG. A low-voltage step-down transformer is utilized for matching the stator and rotor operating voltages.

III. MATHEMATICAL MODELLING OF THE STUDIED WECS

In this section, we demonstrate a comprehensive mathematical modelling of the whole studied system, which includes a WT, DFIG, and a system controlling the WT, RSC, and GSC.

A. Wind Turbine Model

The output mechanical power (P_m) for a VSWT is given by

(1) [11]:

$$P_m = 0.5\rho\pi r^2 C_p(\lambda, \beta) V_w^3 \quad (1)$$

In (1), ρ is the air density; r is the radius of the rotor blade; C_p is the power conversion efficiency of the turbine; β is the blade pitch angle; λ is the tip speed ratio (TSR); and V_w is the wind speed. The TSR (λ) of a WT is derived from (2) [11]:

$$\lambda = \frac{\omega_m r}{V_w} \quad (2)$$

In (2), ω_m denotes the mechanical speed of the rotor. Based on (1) and (2), the mechanical torque (T_m) generated by a WT is represented by (3):

$$T_m = \frac{P_m}{\omega_m} = 0.5\rho\pi r^2 \frac{C_p(\lambda, \beta)}{\lambda} V_w^2 \quad (3)$$

The approximated value of C_p can be computed by (4) and (5) [11]:

$$C_p(\lambda, \beta) = k_1 \left(\frac{k_2}{\gamma} - k_3\beta - k_4\beta^{k_5} - k_6 \right) e^{-\frac{k_7}{\gamma}} \quad (4)$$

$$\gamma = \left(\frac{1}{\lambda + 0.08\beta} - \frac{0.035}{\beta^3 + 1} \right)^{-1} \quad (5)$$

The coefficients k_1 – k_7 can be different to various turbines, depending on the WT rotor and blade design.

B. Modelling of a DFIG

The dynamic model of a DFIG is derived entirely in a synchronous (dq) rotating reference frame [13]. The stator and rotor voltage equations are derived as (6) and (7) [13]:

$$\vec{v}_s^a = R_s \vec{i}_s^a + \frac{d\vec{\psi}_s^a}{dt} + j\omega_s \vec{\psi}_s^a \quad (6)$$

$$\vec{v}_r^a = R_r \vec{i}_r^a + \frac{d\vec{\psi}_r^a}{dt} + j(\omega_s - \omega_m) \vec{\psi}_r^a \quad (7)$$

In (6) and (7), the subscript a denotes the space vectors referred to a synchronously rotating frame (dq); R_s and R_r are the stator and rotor winding resistances, respectively; v_s and v_r denote the stator and rotor voltage space vectors, respectively; i_s and i_r denote the stator and rotor current space vectors, respectively; ψ_s and ψ_r are the stator and rotor flux space vectors, respectively; ω_s and ω_r denote the stator and rotor angular frequencies, respectively.

C. Maximum Power Point Tracking and Pitch Angle Control Systems

Maximum power point tracking (MPPT) controller assists the WECS to harvest the maximum possible power from wind. The generator torque is chosen as to follow a quadratical relationship with the rotational speed (ω_r) [13]. In this model, for MPPT tracking, the following relationship (8) is established:

$$T_{e-ref} = k_m \omega_r^2 - F \omega_r - D \quad (8)$$

In (8), k_m is the maximum power at base wind speed and F and D are the coefficients of the losses.

A pitch angle controller permits the WT to regulate the rotor blade angle to control its power conversion efficiency

synchronization, owing to the mounting of the rotor position sensor and is taken as 30° in this study. The null q -axis grid voltage (v_{qg}) is considered as an indicator of correct sensor position. The rotor angle (θ_r) is referenced to the stator frame and the slip angle (θ_{sl}) for this reference frame transformation is determined as (14). The compensating signal (θ_{cr}) is formed at the output of a PI controller in case of non-zero v_{qg} (14).

$$\left. \begin{aligned} \theta_r &= p\theta_m - \theta_e + \theta_{cr} \\ \theta_{sl} &= \theta_s - \theta_r \end{aligned} \right\} \quad (14)$$

In (14), p denotes the number of pole pairs.

B. Rotor-side Crowbar (RSCB)

To keep the RSC safe from over-currents, crowbar protections are designed. Traditionally, when an abnormal situation is detected, the crowbar is triggered by putting the RSC isolated [10]; its operation is successful in mitigating the transient rotor over-currents. However, during the crowbar activation, the controllability of the DFIG is lost because the rotor-side crowbar short-circuits the rotor windings under grid faults. In this way, the DFIG behaves as a standard induction generator and absorbs a large amount of reactive power.

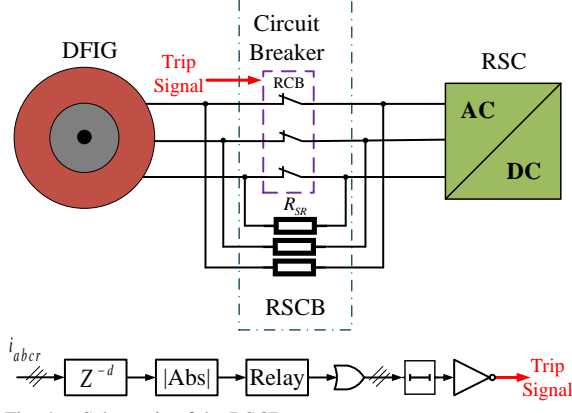


Fig. 4. Schematic of the RSCB.

In this study, an RCB is deployed in series with the rotor and the RSC, and rotor resistors (R_{SR}) are inserted in parallel with the RCB. Under normal operation, the RCB stays connected in the circuit. However, when a fault occurs, the RCB turns-off and the rotor current starts to flow through R_{SR} to limit the fault current. The advantage of this arrangement (Fig. 4) is the uninterrupted control over the DFIG even under abnormal conditions. The value of R_{SR} is calculated as (15):

$$R_{SR} = nR_r \quad (15)$$

In (15), n is a multiple of rotor resistance (R_r).

C. DC-link Crowbar (DLCB)

The main purpose of ESD integration is to improve the stability [15] and reliability of the power system through active power regulation. In this work, a nickel-metal-hydrate battery is taken as an ESD. Nevertheless, this study concentrates only the application of an ESD to enhance the LVRT capability of a DFIG-based WECS.

The proposed control scheme for a DLCB and the control system for an ESD are illustrated in Fig. 5. The ESD control system comprises dual PI regulators in a cascaded structure for

voltage and current loops that are responsible for determining the DC-link voltage (V_{dc}) and ESD current (i_{bat}), respectively. The ESD manages the DC-link to guarantee a constant and reliable DC voltage. The resistor (R_{DC}) keeps the DC-link safe from over-voltages by dissipating extra charge through it. During abnormal condition, the switch S2 activates and dissipates energy through R_{DC} . The value of R_{DC} is selected through a trial-and-error approach, as in [5] by considering the necessary condition of DC-link voltage variations that it must be within the range of 15% of its reference value (16) [1], [8] in defining the value of R_{DC} and the selected value is 0.1Ω .

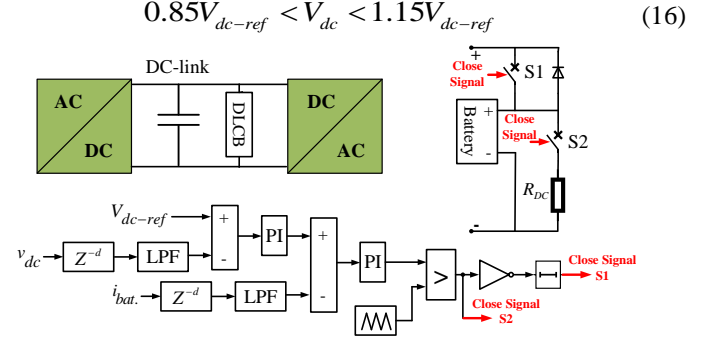


Fig. 5. Schematic of the DLCB.

V. SIMULATION RESULTS AND ANALYSES

This section focuses on the efforts to verify the effectiveness of the proposed schemes for grid integration and enhancement of LVRT capabilities of a DFIG-based WECS during severe and asymmetrical grid voltage dips, respectively. The DFIG parameters are taken from [16], and numerical simulations of the studied system are performed in Simulink/Matlab. It is supposed that the DFIG accelerates with a turned-off stator, and the pitch angle is equal to zero. A wind profile (Fig. 6(a)) is applied to the system under the test which includes both underrated and overrated wind speeds.

A. Startup Inrush Currents

At the start of the simulation, the stator is disconnected from grid as the SCB is turned-off, and the RSC produces the rotor current, i.e. i_{qr-ref} , whereas the rotor d -axis current (i_{dr-ref}) is zero. The GSC is responsible for keeping the net DC-link voltage across the capacitor at the desired level, i.e. 400V in this study. Figure 6(b) shows that rotor speed varies in accordance with wind speeds. The SCB turns-on without attaining positive generator torque, as indicated in Fig. 6(c). Figure 6(d) depicts that the DC-link voltage is maintained at its reference value, which verifies the effectiveness of the designed regulators. Figures 6(e)–(f) show a specified period of stator and rotor currents, respectively, at the instant when the SCB turns-on. Synchronization time depends on initial wind speed. In this study, it takes 5.5s to close the SCB. It can be realized from Fig. 6 that the integration of the DFIG to the utility grid is made without traceable stator and rotor inrush currents.

The same test system is simulated again to highlight the system behavior after ignoring the last two conditions, as described in (13) and the obtained results are presented in Fig. 7. It can be observed from the results that although, the SCB

closes earlier (0.85s) but the significant stator and rotor inrush currents are present in comparison to those obtained in Figs. 6(e)–(f), respectively.

The simulation results concluded that the proposed synchronization method effectively controls the system so as to connect the DFIG with the grid safe and stable and avoids the problem associated with the startup inrush currents.

B. Performance of the proposed LVRT enhancement scheme for symmetrical three-phase fault

This subsection is dedicated to exhibiting the performance of the proposed scheme for enhancing the LVRT capability of a DFIG. A three-phase symmetric fault is applied for 100ms at the time of 12s. Figures 8(a)–(f) show the simulation results of grid-side voltage, grid-side current, generator torque, DC-link voltage, stator current, and rotor current, respectively.

During a fault, the grid-side voltage drops to 10%, which can be seen in Fig. 8(a), and the grid-side current rises accordingly (Fig. 8(b)). With the proposed scheme, the stator and rotor currents are almost 1.5 times higher than their normal values, respectively, which can be seen in Figs. 8(e)–(f), respectively. Consequently, there is no possibility of RSC

over-currents during the voltage dips as the activation of RSCB and DLCB provide relief in mitigating the temporary transients. From the Fig. 8(d), it is obvious that the DC-link voltage remains consistent within the limits (16).

C. Performance of the proposed LVRT enhancement scheme for asymmetrical fault

A single-phase to ground fault is applied at the same aforementioned operating conditions to verify the performance of the proposed scheme. Figure 9(a) shows that the grid-side voltage drops to 15% of its normal operating value. The variations of the selected simulation results (Fig. 9) are higher as compared to symmetrical faults because of higher DC stator flux linkage [3]. From the results, it can be inferred that the proposed control scheme is also effective for asymmetrical grid faults.

It is apparent from the simulation results that when an abnormality is sensed, the ESD is activated for mitigating transient EMF and keeps the DC-link voltage in safe limits. Under such circumstances, we can conclude that the proposed control scheme is capable to fulfill the LVRT requirements.

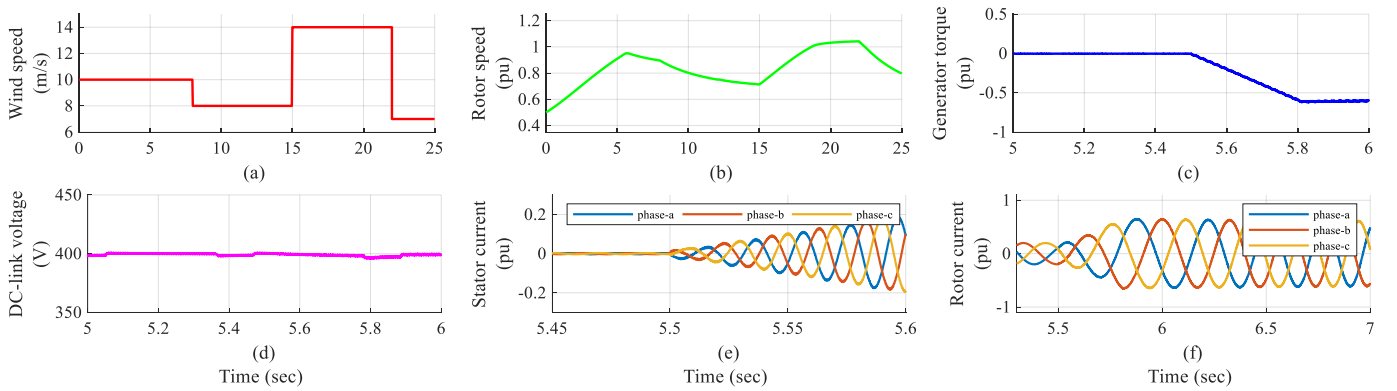


Fig. 6. Simulation results during startup process: a) wind speed, b) rotor speed, c) generator torque, d) DC-link voltage, e) stator current, and f) rotor current.

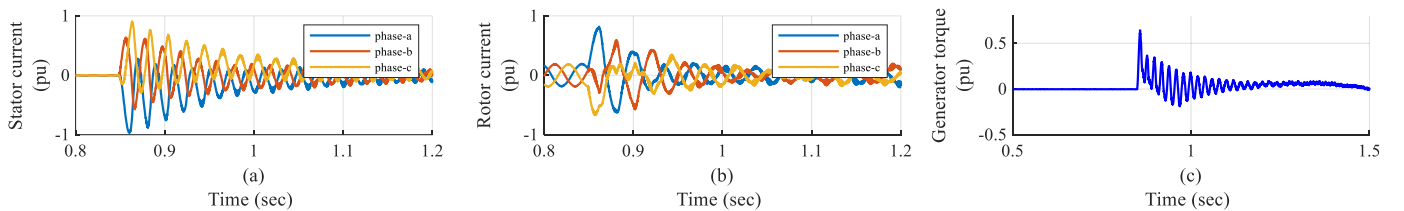


Fig. 7. Simulation results obtained during startup process by conventional method: a) stator current, b) rotor current, and c) generator torque.

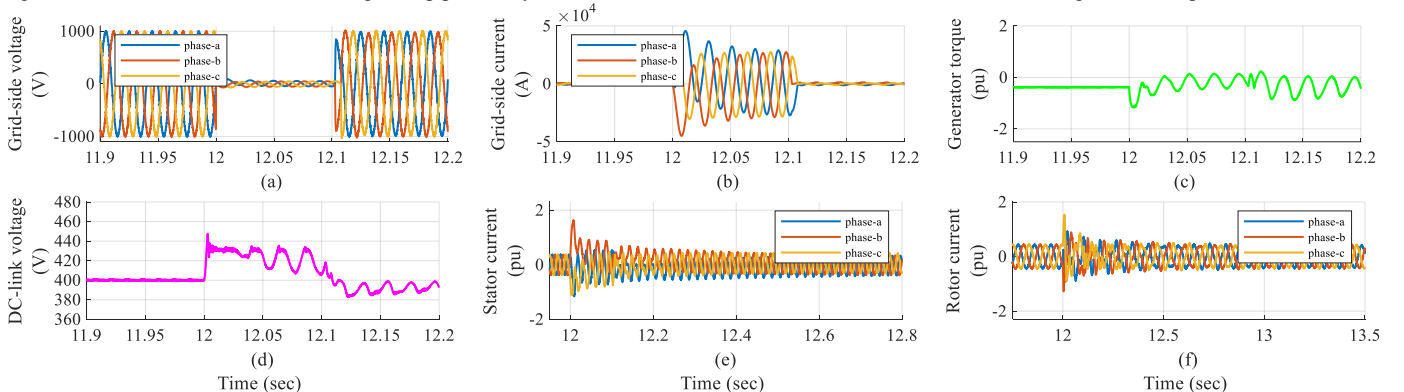


Fig. 8. Simulation results for symmetrical voltage dips: a) grid-side voltage, b) grid-side current, c) generator torque, d) DC-link voltage, e) stator current, and f) rotor current.

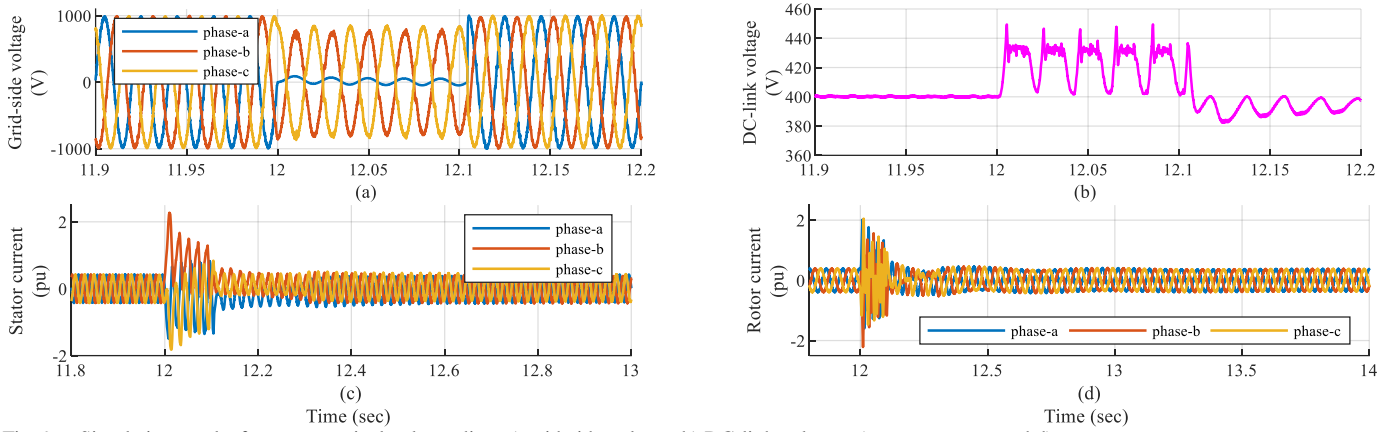


Fig. 9. Simulation results for asymmetrical voltage dips: a) grid-side voltage, b) DC-link voltage, c) stator current, and d) rotor current.

Finally, a comparison of the proposed DLCB method is made with a DC chopper. It is one of the most-used hardware solution for DFIG-based WECS to enhance its LVRT capability for grid faults [13], [14]. A DC chopper is an electric device connected in parallel to the DC bus to prevent DC-link over-voltages [14]. Keeping all the system parameters and limitations similar, the test system is simulated for both symmetrical and asymmetrical grid faults and the obtained results are shown in Fig. (10). From the results, we can conclude that with the aid of the proposed DLCB method, the test system performs very well in mitigating the DC-link over-voltages in comparison to a DC chopper, thus ensuring the superiority of the proposed method.

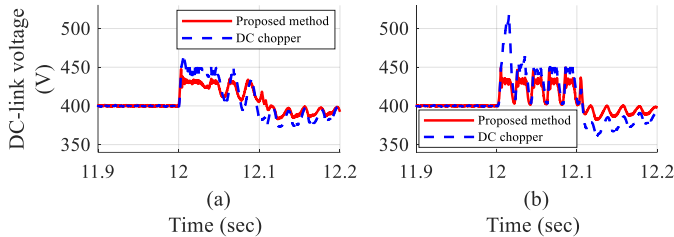


Fig. 10. Comparative results: a) symmetrical, b) asymmetrical voltage dips.

VI. CONCLUSIONS

In this paper, the synchronization problem of a DFIG-based WECS with the grid, and the rotor over-currents and DC-link voltage fluctuations during grid faults were discussed.

This study presented a synchronization method of grid-connection and the simulation results verified its effectiveness to suppress the startup inrush currents.

A combination of a rotor-side crowbar and an ESD-based DC-link crowbar was incorporated to mitigate the rotor over-currents and DC-link voltage fluctuations. The results confirmed that this combination effectively controlled DC-link variations and limited over-current transients during grid faults. Thus, it can be concluded that the proposed control scheme enhanced the LVRT capability of a DFIG-based WECS and improved the system stability and reliability.

VII. REFERENCES

- [1] Y. Shen, D. Ke, Y. Sun, D. S. Kirschen, W. Qiao, and X. Deng, "Advanced Auxiliary Control of an Energy Storage Device for Transient Voltage Support of a Doubly Fed Induction Generator," *IEEE Trans. Sustain. Energy*, vol. 7, no. 1, pp. 63-76, Jan. 2016.
- [2] G. Rashid, and M. H. Ali, "Nonlinear Control-Based Modified BFCL for LVRT Capacity Enhancement of DFIG-Based Wind Farm," *IEEE Trans. Energy Convers.*, vol. 32, no. 1, pp. 284-295, March 2017.
- [3] S. Xiao, G. Yang, H. Zhou, and H. Geng, "An LVRT Control Strategy Based on Flux Linkage Tracking for DFIG-Based WECS," *IEEE Trans. Ind. Electron.*, vol. 60, no. 7, pp. 2820-2832, July 2013.
- [4] Y. M. Alsmadi, L. Xu, F. Blaabjerg, A. J. P. Ortega, A. Y. Abdelaziz, A. Wang, and Z. Albatineh, "Detailed Investigation and Performance Improvement of the Dynamic Behavior of Grid-Connected DFIG-Based Wind Turbines Under LVRT Conditions," *IEEE Trans. Ind. Appl.*, vol. 54, no. 5, pp. 4795-4812, Sept.-Oct. 2018.
- [5] A. M. A. Haidar, K. M. Muttaqi, and M. T. Hagh, "A Coordinated Control Approach for DC link and Rotor Crowbars to Improve Fault Ride-Through of DFIG-Based Wind Turbine," *IEEE Trans. Ind. Appl.*, vol. 53, no. 4, pp. 4073-4086, July-Aug. 2017.
- [6] X. Li, X. Zhang, Z. Lin, and Y. Niu, "An Improved Flux Magnitude and Angle Control With LVRT Capability for DFIGs," *IEEE Trans. Power Systems*, vol. 33, no. 4, pp. 3845-3853, July 2018.
- [7] H. Geng, C. Liu, and G. Yang, "LVRT Capability of DFIG-Based WECS Under Asymmetrical Grid Fault Condition," *IEEE Trans. Ind. Electron.*, vol. 60, no. 6, pp. 2495-2509, June 2013.
- [8] D. Xie, Z. Xu, L. Yang, J. Østergaard, Y. Xue, and K. P. Wong, "A Comprehensive LVRT Control Strategy for DFIG Wind Turbines With Enhanced Reactive Power Support," *IEEE Trans. Power Systems*, vol. 28, no. 3, pp. 3302-3310, Aug. 2013.
- [9] L. Zhou, J. Liu, and S. Zhou, "Improved Demagnetization Control of a Doubly-Fed Induction Generator Under Balanced Grid Fault," *IEEE Trans. Power Electron.*, vol. 30, no. 12, pp. 6695-6705, Dec. 2015.
- [10] A. Jalilian, S. B. Naderi, M. Negnevitsky, M. Tarafdard Hagh, and K. M. Muttaqi, "Controllable DC-link fault current limiter augmentation with DC chopper to improve fault ride-through of DFIG," *IET Renew. Power Gener.*, vol. 11, no. 2, pp. 313-324, 8 2017.
- [11] M. Firouzi, and G. B. Gharehpetian, "LVRT Performance Enhancement of DFIG-Based Wind Farms by Capacitive Bridge-Type Fault Current Limiter," *IEEE Trans. Sustain. Energy*, vol. 9, no. 3, pp. 1118-1125, July 2018.
- [12] Y. Kailasa Gounder, D. Nanjundappan, and V. Boominathan, "Enhancement of transient stability of distribution system with SCIG and DFIG based wind farms using STATCOM," *IET Renew. Power Gener.*, vol. 10, no. 8, pp. 1171-1180, 9 2016.
- [13] G. Abad, J. Lopez, M. A. Rodriguez, L. Marroyo, and G. Iwanski, *Doubly Fed Induction Machine: Modeling and Control for Wind Energy Generation*, New York: Wiley, 2011, p. 214, 20, 199, 492.
- [14] D. Xu, F. Blaabjerg, W. Chen, and N. Zhu, *Advanced Control of Doubly Fed Induction Generator for Wind Power Systems*, IEEE Press: Wiley, 2018, p. 99-101, 25, 367.
- [15] M. A. S. Ali, K. K. Mehmood, J. K. Park, C. H. Kim, "Battery Energy Storage System-Based Stabilizers for Power System Oscillations Damping," *Journal of the Korean Institute of Illuminating and Electrical Installation Engineers*, vol. 10, pp. 75-84, Oct. 2016.
- [16] B. Wu, Y. Lang, N. Zargari, S. Kouro, *Power Conversion and Control of Wind Energy Systems*, John Wiley & Sons, Inc., Hoboken, NJ, USA, 2011, p. 322.